



THE UNIVERSITY *of* EDINBURGH

Edinburgh Research Explorer

Complex multi-decadal ice dynamical change inland of marine-terminating glaciers on the Greenland Ice Sheet

Citation for published version:

Williams, J, Gourmelen, N & Nienow, P 2021, 'Complex multi-decadal ice dynamical change inland of marine-terminating glaciers on the Greenland Ice Sheet', *The Journal of Glaciology*, pp. 1-14.
<https://doi.org/10.1017/jog.2021.31>[Opens in a new window]

Digital Object Identifier (DOI):

[10.1017/jog.2021.31](https://doi.org/10.1017/jog.2021.31)[Opens in a new window]

Link:

[Link to publication record in Edinburgh Research Explorer](#)

Document Version:

Publisher's PDF, also known as Version of record

Published In:

The Journal of Glaciology

Publisher Rights Statement:

© The Author(s), 2021. Published by Cambridge University Press.

General rights

Copyright for the publications made accessible via the Edinburgh Research Explorer is retained by the author(s) and / or other copyright owners and it is a condition of accessing these publications that users recognise and abide by the legal requirements associated with these rights.

Take down policy

The University of Edinburgh has made every reasonable effort to ensure that Edinburgh Research Explorer content complies with UK legislation. If you believe that the public display of this file breaches copyright please contact openaccess@ed.ac.uk providing details, and we will remove access to the work immediately and investigate your claim.





Article

Cite this article: Williams JJ, Gourmelen N, Nienow P (2021). Complex multi-decadal ice dynamical change inland of marine-terminating glaciers on the Greenland Ice Sheet. *Journal of Glaciology* 1–14. <https://doi.org/10.1017/jog.2021.31>

Received: 9 December 2020

Revised: 19 February 2021

Accepted: 22 February 2021

Keywords:

Arctic glaciology; atmosphere-ice-ocean interactions; glacier flow; ice dynamics

Author for correspondence:

Joshua J. Williams,

Email: j.j.williams-4@sms.ed.ac.uk

Complex multi-decadal ice dynamical change inland of marine-terminating glaciers on the Greenland Ice Sheet

Joshua J. Williams , Noel Gourmelen and Peter Nienow

School of Geosciences, University of Edinburgh, Edinburgh, EH8 9XP, UK

Abstract

Greenland's future contribution to sea-level rise is strongly dependent on the extent to which dynamic perturbations, originating at the margin, can drive increased ice flow within the ice-sheet interior. However, reported observations of ice dynamical change at distances $> \sim 50$ km from the margin have a very low spatial and temporal resolution. Consequently, the likely response of the ice-sheet's interior to future oceanic and atmospheric warming is poorly constrained. Through combining GPS and satellite-image-derived ice velocity measurements, we measure multi-decadal (1993–1997 to 2014–2018) velocity change at 45 inland sites, encompassing all regions of the ice sheet. We observe an almost ubiquitous acceleration inland of tidewater glaciers in west Greenland, consistent with acceleration and retreat at glacier termini, suggesting that terminus perturbations have propagated considerable distances (> 100 km) inland. In contrast, outside of Kangerlussuaq, we observe no acceleration inland of tidewater glaciers in east Greenland despite terminus retreat and near-terminus acceleration, and suggest propagation may be limited by the influence of basal topography and ice geometry. This pattern of inland dynamical change indicates that Greenland's future contribution to sea-level will be spatially complex and will depend on the capacity for dynamic changes at individual outlet glacier termini to propagate inland.

1. Introduction

The Greenland Ice Sheet (GrIS) has lost mass to the ocean at an increasing rate over recent decades (Rignot and others, 2008, 2011; Shepherd and others, 2012, 2020; Enderlin and others, 2014; King and others, 2018; Mouginot and others, 2019), and now has the largest contribution to global sea-level rise of any individual ice body (Vaughan and others, 2013; Bamber and others, 2018). Estimates indicate that ~ 48 –66% of this mass loss can be attributed to glacier dynamics, with this dynamic loss driven by the acceleration and retreat of marine-terminating glaciers and increasing by 14% between 1985–1999 and 2007–2018 (King and others, 2020), and the remaining ~ 34 –52% due to surface mass balance (SMB) (Mouginot and others, 2019; Shepherd and others, 2020). Following a step-increase in ice discharge in the early-2000s, the GrIS is suggested to have entered a state of persistent mass loss (King and others, 2020), and recent model intercomparison work projects a future sea-level rise contribution of 32 ± 17 to 90 ± 50 mm by 2100 (Goelzer and others, 2020). Almost all of our current observations of long-term change are concentrated at the margins of the ice sheet, which have been characterised by thinning (Pritchard and others, 2009; McMillan and others, 2016; Sørensen and others, 2018) and both substantial velocity accelerations (Rignot and Kanagaratnam, 2006; Joughin and others, 2010, 2018; Moon and others, 2012) and near-ubiquitous retreat of marine-terminating outlet glaciers (Murray and others, 2015; Bunce and others, 2018), especially in the northwest and southeast.

In contrast, our understanding of changes in the dynamics of inland regions of the ice sheet is far more limited, and yet any such changes would be important for several reasons. At land-terminating margins, while the impacts of variable hydrological forcing on ice flow have been well-studied near the ice margin (van de Wal and others, 2008, 2015; Bartholomew and others, 2010; Sole and others, 2013; Tedstone and others, 2015), it remains unclear whether meltwater can access the bed, and efficient subglacial channels form, further into the ice-sheet interior where the ice is thicker and rates of surface melting are lower (Nienow and others, 2017). This is particularly important given that as the ELA rises in response to projected increases in surface melt (Hanna and others, 2008), the area of the ice-sheet surface undergoing melt will increase exponentially due to the hypsometry of the ice-sheet surface (Bartholomew and others, 2011; Machguth and others, 2016). Furthermore, some studies have postulated that ice motion will scale positively with surface melting at high elevations (Doyle and others, 2014; Gagliardini and Werder, 2018), and others that the presence of liquid water within the englacial hydrological system may increase ice deformation rates over time scales of years to decades (Phillips and others, 2010, 2013). More generally, considering conservation of mass, the thickness of ice in the interior is considerably greater than that at the margin, and so any increase in ice motion has the potential to result in a much larger increase in mass flux when compared to marginal regions (Doyle and others, 2014), particularly for marine-terminating margins which are characterised by faster flow velocities and can

discharge any increase in mass flux directly into the ocean. As a consequence, future sea-level change projections are strongly dependent on how quickly mass can be transported from the ice-sheet interior to the margin (Price and others, 2008, 2011; Felikson and others, 2017, 2020), as well as the time required for the ice sheet to reach a new steady-state following a perturbation. For example, modelling work indicates that ~75% of the projected sea-level rise from Greenland, which would result from the response of the ice sheet to forcing over the past few decades, is yet to come (Price and others, 2011). Furthermore, additional estimates suggest thinning may continue for hundreds (Wang and others, 2012) to thousands (Price and others, 2008) of years until a new steady-state is reached.

Several mechanisms have been proposed to drive a change in the ice dynamics within regions inland of Greenland's tidewater glacier termini. Changes to the surface slope and thickness of the ice, as a result of ice dynamical and/or SMB change, impact upon the driving stress, in turn affecting the rates of ice flow through internal deformation of the ice (Cuffey and Paterson, 2010). Such a change in driving stress, and thus internal deformation, can be driven through the up-glacier propagation of changes at the terminus of tidewater glaciers (i.e. Howat and others, 2008; Price and others, 2008, 2011; Nick and others, 2009; Felikson and others, 2017, 2020); for example, the loss of back-stress as a result of the loss of a floating ice tongue, or an increase in strain rate as the terminus retreats into deeper water (Price and others, 2011). This perturbs the force-balance, and the resultant acceleration leads to thinning of nearby upstream ice, steepening the local glacier surface thereby increasing the driving stress, resulting in further acceleration causing thinning and acceleration to propagate upstream (Nick and others, 2009). The propagation of this thinning can be modelled as a diffusive kinematic wave (Nye, 1960, 1963; Nick and others, 2009; Price and others, 2011; Felikson and others, 2017, 2020). This process can initiate a dramatic change in inland velocities, as observed during large 'surging' events at some Arctic ice caps (i.e. McMillan and others, 2014; Willis and others, 2018; Zheng and others, 2019).

Recent work (Felikson and others, 2017, 2020) suggests there may be geometrical constraints on the ability for thinning (and thus velocity) perturbations to propagate inland. These studies calculate the Péclet number (Pe), which describes the ratio of the rate at which a kinematic wave diffuses upstream or advects downstream. A threshold value of $Pe = 3$ is argued to represent the location at which 89% of dynamic change has occurred (Felikson and others, 2020), thus offering a possible empirical threshold by which to measure the ability of changes at the margin to propagate inland. Through applying this to 141 tidewater glaciers across the GrIS, Felikson and others (2020) suggest two end-member geometries describe those glaciers with the greatest potential for dynamic mass loss; those with a relatively low mass flux but with basal topography permitting thinning to diffuse far inland (i.e. northwest Greenland), and those with high mass flux but with thinning limits close to the margin (i.e. southeast Greenland).

In spite of the wealth of studies, there is little observational data to constrain these theoretical and model results, especially at higher elevations further inland. Direct observations of velocity change inland of fast-flowing marine-terminating outlet glaciers are limited to sparse GPS measurements of seasonal flow variations at a few individual glaciers (Sole and others, 2011; Ahlström and others, 2013), and a single long-term (multi-decadal) study observing changes in ice motion extending ~80–100 km from the grounding line at Zachariae Isstrøm in northeast Greenland (Mouginot and others, 2015). Recent measurements of mass change from ICESat and ICESat-2 show thinning extending

inland to elevations of 2000–2500 m (a.s.l.) in western and southern Greenland, particularly inland of Jakobshavn Isbrae and tide-water glaciers in the northwest, and to 1500 m (a.s.l.) in northeast Greenland (Smith and others, 2020), although thinning is the result of both dynamic change and changes in SMB. To disentangle the relative contribution of dynamic and SMB, thereby isolating the dynamic signal of mass loss, surface elevation change (SEC) can be corrected with SMB fields derived from regional climate models (Pritchard and others, 2009; Zwally and others, 2011; McMillan and others, 2016; Felikson and others, 2017). The majority of pronounced dynamic thinning is found in a relatively narrow set of regions; Jakobshavn Isbrae, Upernavik Isstrøm and Steenstrup Glacier on the west coast, Kangerlussuaq in the southeast, and Zachariae Isstrøm in the northeast (McMillan and others, 2016). While dynamic thinning has been observed to penetrate inland of fast-flowing outlet glaciers (Pritchard and others, 2009; Zwally and others, 2011; McMillan and others, 2016), the amplitude of thinning from a small perturbation in ice velocity is expected to be well below the combined uncertainty of altimetry and SMB models and so the inland limit of dynamic thinning comes with large uncertainty. Consequently, there is a need for additional robust measurements of dynamics, and thus potentially dynamic change, within the accumulation zone of the GrIS in order to quantify how the interior of the GrIS has responded to climate warming and associated ice marginal dynamic perturbations.

During the period 1993–1997, a line of 161 stakes located ~30 km apart was installed in a 'girdle' around the entire GrIS at ~2000 m elevation as part of the NASA-led Program for Arctic Regional Climate Assessment (PARCA) project, in order to estimate the mass balance of the ice-sheet interior (Thomas and others, 1998, 2000, 2001). At each stake, annual ice velocity was calculated using GPS observations recorded over a 1-year return period sometime between 1993 and 1997. This period was characterised by stable mass balance (Sørensen and others, 2018) and preceded both the recent rapid acceleration in ice motion observed at many of Greenland's marine-terminating outlet glaciers (Thomas and others, 2003; Joughin and others, 2004; Luckman and others, 2006; Holland and others, 2008; Murray and others, 2010; Bevan and others, 2012; Hill and others, 2018), and the slowdown in the southwest land-terminating sector (Tedstone and others, 2015; van de Wal and others, 2015; Stevens and others, 2016; Williams and others, 2020), which both began in the late-1990s to early-2000s. While inland velocity measurements have previously been limited to GPS data, the launch of Landsat-8 in 2013, among other advances in satellite imaging, has led to the extension of large-scale feature tracking into the ice-sheet interior (Fahnestock and others, 2016; Gardner and others, 2018, 2019). Since 2013, some marine-terminating glaciers have continued to accelerate while others have stabilised or slowed down (Joughin and others, 2018, 2020; Lemos and others, 2018; Khazendar and others, 2019; Mankoff and others, 2020). Few, however, have remained stable since the 1990s or returned to speeds comparable to those prior to the initial acceleration (Bevan and others, 2012; Joughin and others, 2018).

Here, we compare recent satellite-image-derived velocities in the ice-sheet interior to those collected at the PARCA GPS stakes along the 2000 m elevation contour in the mid-1990s to quantify how the interior of the GrIS has responded to the period of dramatic change observed at marine-terminating margins of the GrIS during the 2000s and 2010s. We measure multi-decadal ice velocity change at 45 sites inland of tidewater margins, encompassing all regions of the ice sheet. Subsequently, we assess the observed pattern of change with respect to the patterns of velocity change at the margins, ice geometrical constraints and modelled SMB from MAR v3.10 (Fettweis and others, 2017).

2. Data and methods

2.1 PARCA ice velocities around the 2000 m traverse

The PARCA dataset consists of GPS receivers at 161 stakes, located ~30 km apart and spanning the entire 2000 m elevation contour of the GrIS, except for the southwest where the stakes were placed at higher elevations to avoid nunataks, mountains and crevasses (Thomas and others, 1998, 2000). At each GPS station, an annual ice velocity (m a^{-1}) was recorded within the period 1993–1997, as well as surface elevation (m a.s.l.) and ice thickness (m), the latter of which was measured by ice-penetrating radar. The precision of annual velocity measurements from these GPS sites is $<0.5 \text{ m a}^{-1}$, and better than 0.2 m a^{-1} in most cases (Thomas and others, 1998). We apply a conservative uncertainty of $\pm 0.5 \text{ m a}^{-1}$ at all sites.

It should be noted that while the GPS sites are located at approximately the same surface elevation, there are considerable differences in the distance from their respective glacier termini (Fig. S6), with a notable increase in distance inland in the north and northeast.

2.2 NASA MEaSUREs ITS-LIVE ice velocities

Recent advances in satellite imaging have enabled the routine mapping of ice velocities (Dehecq and others, 2015; Fahnestock and others, 2016), with enhanced coverage in the interiors of the ice sheets (Gardner and others, 2018). Here, we use the NASA MEaSUREs ITS-LIVE annual velocity mosaics (v0) of the GrIS, generated from Landsat imagery through the auto-RIFT feature tracking processing chain (Gardner and others, 2018), covering the period 1985–2018 and gridded to 240 m (Gardner and others, 2019). Full documentation of this dataset is available from <https://its-live.jpl.nasa.gov/#documentation>. We use this dataset as the ice velocity measurements extend to the 2000 m elevation contour and both effective pair length (dt) and centre date are provided at each pixel such that we can assess the impact of any seasonality introduced in our analyses. Moreover, a recent assessment of satellite-image-derived ice velocities within the Greenland interior shows that when compared to GPS velocities from 2015 to 2019, located ~150 km from the ice divide in the Northeast Greenland Ice Stream (NEGIS; $75^{\circ}38\text{N}$, $35^{\circ}60\text{W}$), ITS-LIVE velocities from 2013 to 2018 are characterised by the lowest bias (0.31 m) of all velocity products assessed (Hvidberg and others, 2020). For the calculation of multi-decadal ice velocity change, we use the data spanning 2014–2018, produced from Landsat-8 imagery. While Landsat-8 imagery was used to compute the 2013 velocity field, it was used in conjunction with Landsat-7 imagery, and so the uncertainties are much higher than for 2014–2018 given the lower radiometric resolution of Landsat-7 compared to Landsat-8. Given the slow ice speeds within the interior, any such uncertainty can make up a considerable part of the observed change, hence we do not include data earlier than 2014 in our analyses.

2.3 ITS-LIVE velocity extraction at PARCA GPS sites

Prior to velocity extraction, we exclude pixels with a velocity below 10 m a^{-1} , reasoning that the associated uncertainties constitute an unacceptably high percentage at very low velocities. Following this thresholding, we extract ice velocity (m a^{-1}), ice velocity uncertainty (m a^{-1}), effective pair length (days) and effective centre date from a 3×3 -pixel ($720 \times 720 \text{ m}$) window around each of the 161 PARCA GPS sites, taking the median value of each from the extracted window. We repeat this for each year in the period 2014–2018, and then calculate the median velocity and uncertainty across the 2014–2018 period (calculated from whichever years we have data at a given GPS site) to account for any year-to-year variability in ice velocity.

Seasonal variability in ice velocities has been observed near the margins of tidewater glaciers in Greenland (Lemos and others, 2018), as well as up to at least ~70 km inland at Kangiata Nunaata Sermia in southwest Greenland (Sole and others, 2011) and at an elevation of 1850 m (a.s.l.), 140 km inland in the southwest land-terminating sector (Doyle and others, 2014). We calculate the potential impact of such seasonality on the satellite-image-derived velocity data at the PARCA GPS sites, as described in Supplementary Text 1, and observe no coherent pattern showing any clear evidence of seasonality in the velocity data at these elevations.

2.4 Calculating velocity change

For each GPS site, we use the 2014–2018 median ITS-LIVE velocity to calculate a decadal velocity change through the following:

$$\text{Velocity change (m a}^{-1}\text{)} = \text{ITS_LIVE velocity}_{2014-2018} - \text{GPS velocity}$$

$$\text{Velocity change (\%)} = \frac{\text{ITS_LIVE velocity}_{2014-2018} - \text{GPS velocity}}{\text{GPS velocity}} \times 100$$

It should be noted that for inland regions where the ice is flowing much more slowly than at the margins, any uncertainties in the ice velocity measurements may equal a considerable proportion of any measured velocity change. Following this, we first remove any sites where the measured velocity change (m a^{-1}) is less than or equal to the 2014–2018 median velocity uncertainty (m a^{-1}) extracted from the ITS-LIVE data added to the 0.5 m uncertainty of the GPS measurements (Thomas and others, 1998). To assess temporal variability, at each GPS site, we calculate the std dev. of the annual velocity for the period 2014–2018. We remove any GPS sites where our measured velocity change (2014–2018 median) is less than or equal to the std dev. at that site. The locations of these sites are shown in Figure S7. Following this filtering, we measure decadal velocity change at 45 GPS sites.

At these 45 sites, ITS-LIVE velocity uncertainties range from 0.1 to 11.5 m a^{-1} , with a mean uncertainty of 1.8 m a^{-1} , for the years 2014–2018 (Fig. S8). At the majority of the GPS sites included in our analyses, both median ice velocity uncertainty (m a^{-1}) and the ice velocity std dev. (m a^{-1}) across the 2014–2018 ITS-LIVE data are very low, often $<1\text{--}2 \text{ m a}^{-1}$ (Fig. S8). In addition, almost all of the GPS sites have ITS-LIVE data in all 5 years (2014–2018, Fig. S8D), such that the median velocity and velocity uncertainty are representative of the entire period, thereby limiting any temporal bias.

We observe absolute magnitudes of change ranging from -9.4 ± 3.3 to $+28.1 \pm 8.3 \text{ m a}^{-1}$ (Fig. 1a), and also report these as percentage changes (Fig. 1b). Where there are multiple GPS sites inland of a glacier, we report the range of velocity change values observed across these sites, and we also report the combined ITS-LIVE and GPS uncertainties.

2.5 Velocity time series creation

To compare acceleration in the interior with changes in ice motion at the margins, we create time series of ice velocity at the ice-sheet margin using the full ITS-LIVE dataset from 1985 to 2018 (Gardner and others, 2018, 2019). For each glacier studied, we define an area of interest (AOI) near the terminus. Within this AOI, we then remove pixels that are flowing slower than a specified minimum velocity, as well as pixels with an uncertainty greater

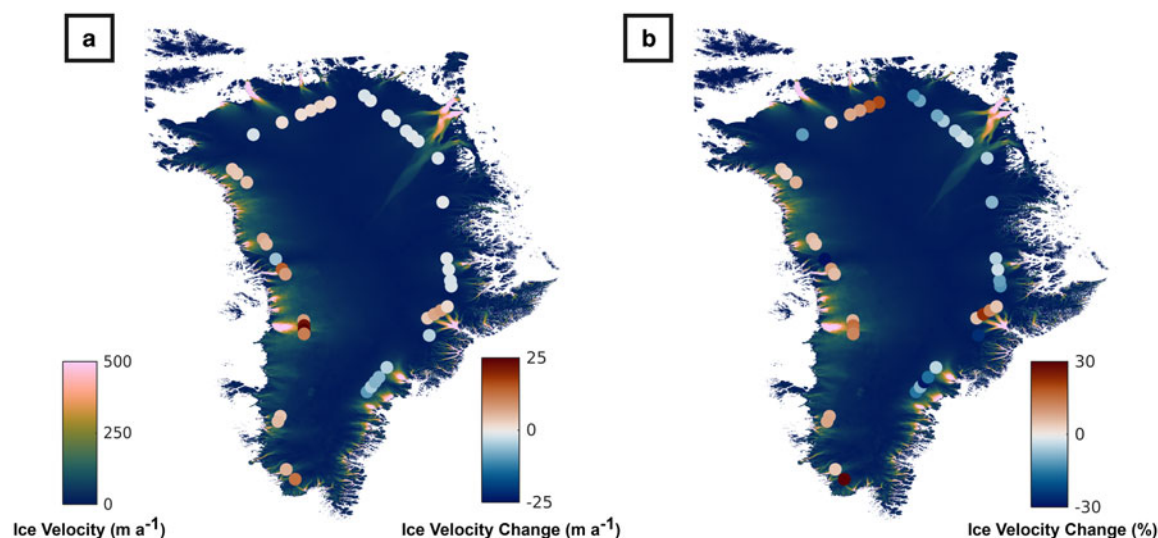


Fig. 1. Ice velocity change (a: m a^{-1} , b: %) at 45 GPS sites inland of tidewater margins between the periods 1993–1997 and 2014–2018. The base image is the 2016 velocity field from the NASA MEaSUREs ITS-LIVE v0 product (Gardner and others, 2018, 2019).

than a specified threshold value, for each year of ITS-LIVE data. These velocity and uncertainty thresholds differ between sites, with full input parameters given in Table S1. We then calculate the pixels common to all years of ITS-LIVE data within the AOI, such that there is no spatial bias influencing the time series. These pixels are shown for each site in Figures S9–S25.

At fast-flowing outlet glaciers, the pair lengths used to compute velocity are often smaller than those further inland where greater temporal separation is necessary to measure displacement given the slower flow speeds. Seasonal velocity variability has been observed at several of Greenland's tidewater glaciers from both GPS measurements (Sole and others, 2011) and satellite remote sensing (Lemos and others, 2018), and may impact upon the extracted velocities and thus time series. As such, we calculate the percentage of summer (JJA) coverage at each common pixel for each year using the centre-date and effective pair length, as described in Supplementary Text 1. We then calculate the median summer coverage across all common pixels for each year of data, and colour-code the scatter points in Figures 2–4 by these values.

2.6 Surface mass balance

Changes in ice motion can be driven by changes in SMB, for example, through meltwater input to the bed (Tedstone and others, 2015), cryo-hydrologic warming (Phillips and others, 2010, 2013) or simply the impact on local driving stress through ice thinning and surface slope change (Tedstone and others, 2015). We obtain SMB data from the MAR v3.10 regional climate model (Fettweis and others, 2017), forced by NCEP-NCARv1 from 1992 to 2019. Modelled melt production and SMB are extracted from a 3-by-3-pixel window around each GPS station, for the years 1990–1999 and 2014–2018. Mean values are calculated for each of these time periods, which are then differenced to calculate the change in modelled melt production and SMB between the GPS and satellite velocity measurement periods.

3. Results

3.1 Multi-decadal velocity change around the 2000 m traverse

We observe a near-ubiquitous acceleration inland of marine-terminating glaciers on the west coast (Fig. 1). Across four GPS sites ~117 km inland of the terminus of Jakobshavn Isbrae, the

largest and fastest flowing outlet glacier of the GrIS (Joughin and others, 2004, 2020; Holland and others, 2008; Khazendar and others, 2019), we observe an acceleration ranging from 7.6 ± 4.2 to $28.1 \pm 7.8 \text{ m a}^{-1}$.

Similarly, we observe accelerations up-glacier from Narsap Sermia (3.6 ± 0.8 to $4.6 \pm 1.6 \text{ m a}^{-1}$) in the southwest, and inland of Rink Isbrae (7.8 ± 2.7 to $14.6 \pm 7.5 \text{ m a}^{-1}$), Upernavik Isstrøm (4.9 ± 1.9 to $6.3 \pm 2.2 \text{ m a}^{-1}$) and Kong Oscar Gletsjer (3.3 ± 1.0 to $3.7 \pm 2.4 \text{ m a}^{-1}$) in central to northwest Greenland. The only glacier where we observe inland deceleration on the west coast is Umiammakku Isbrae ($-5.5 \pm 2.8 \text{ m a}^{-1}$).

North Greenland is characterised by very small changes in inland flow (-1.8 ± 0.7 to $+2.1 \pm 0.8 \text{ m a}^{-1}$), with minor accelerations of $1.1 \pm 0.4 \text{ m a}^{-1}$ and 1.0 ± 0.3 to $2.1 \pm 0.3 \text{ m a}^{-1}$ inland of Petermann Gletsjer and Ryder Gletsjer, respectively. In contrast, the NEGIS (which drains into 79 North Glacier and Zachariae Isstrøm) has seen a slowdown of -1.3 ± 0.7 to $-1.8 \pm 0.6 \text{ m a}^{-1}$. To the north of the NEGIS, Academy Gletsjer also shows inland deceleration (-1.3 ± 0.2 to $-1.8 \pm 0.2 \text{ m a}^{-1}$).

In contrast to west Greenland, interior acceleration has been largely absent from the east coast. In central-east Greenland, the inland region draining into Dagaard-Jensen Gletsjer has decelerated by -1.3 ± 0.4 to $-1.5 \pm 0.3 \text{ m a}^{-1}$. Further south, Kangerlussuaq has a more complex pattern, with a 1.7 ± 0.8 to $7.5 \pm 2.2 \text{ m a}^{-1}$ interior acceleration inland of two of its flow branches, and a $-4.0 \pm 1.9 \text{ m a}^{-1}$ deceleration inland of the most southerly branch. In the southeast, we observe decelerations inland of Helheim Gletsjer (-4.1 ± 1.2 to $-6.8 \pm 1.3 \text{ m a}^{-1}$) and Ikertivaq (-4.9 ± 2.0 to $-9.4 \pm 2.8 \text{ m a}^{-1}$).

We next assess multi-decadal (1985–2018) time series of near-terminus ITS-LIVE ice velocity (Gardner and others, 2018, 2019) downstream of our inland velocity change measurements to investigate whether the observed inland velocity change may be driven by the up-glacier propagation of acceleration at the terminus.

3.2 Near-terminus velocity change

Numerous studies have measured multi-annual ice velocity change near the terminus of Greenland's tidewater glaciers (e.g. Rignot and Kanagaratnam, 2006; Howat and others, 2007, 2008; Joughin and others, 2008, 2010, 2018; Murray and others, 2010; Bevan and others, 2012; Moon and others, 2012; Mouginot and others, 2015). Through assessing ITS-LIVE ice velocity change (Gardner

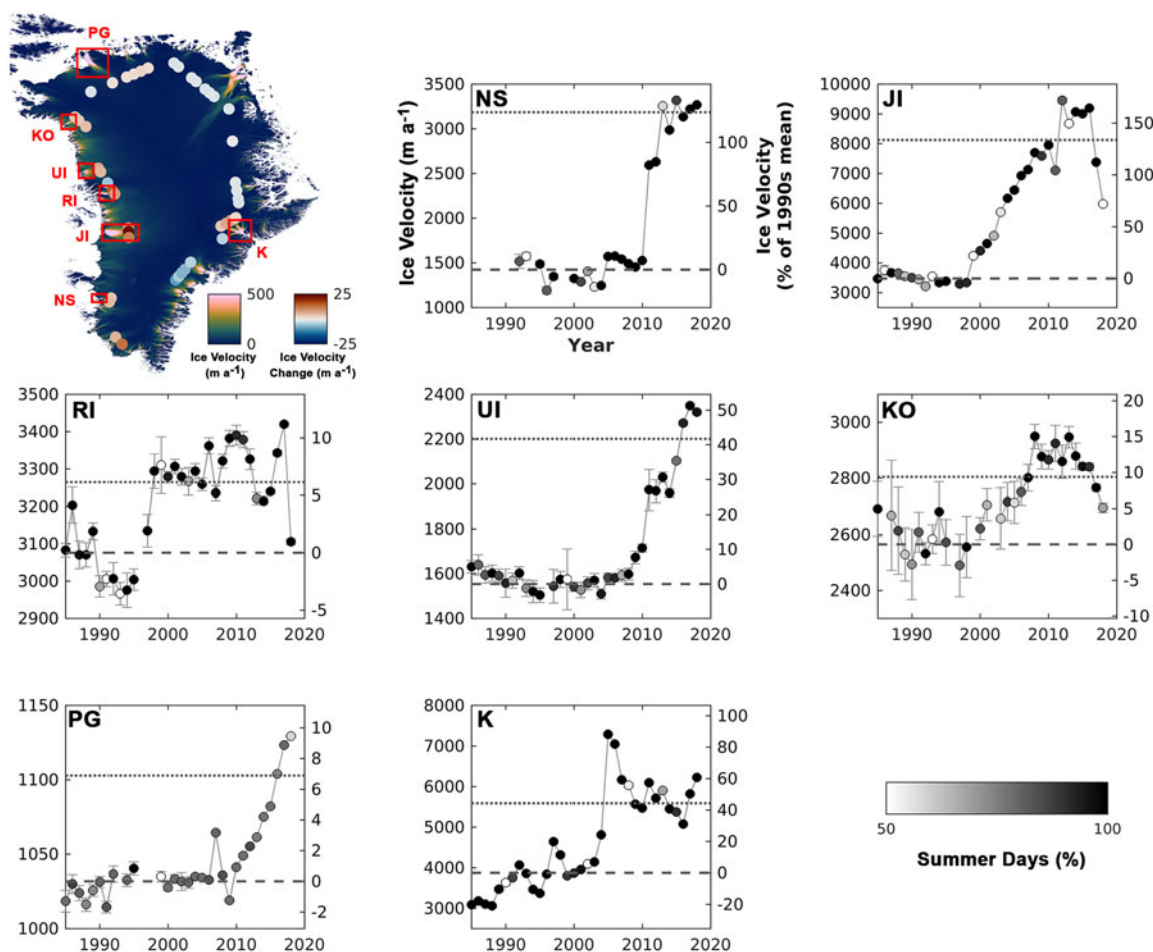


Fig. 2. Time series of ITS-LIVE ice velocity (m a^{-1}) from 1985 to 2018 measured near the terminus (see Supplementary Figs S9–S15 for exact locations) for glaciers inland of which multi-decadal acceleration is observed; (NS) Narsap Sermia, (JI) Jakobshavn Isbrae, (RI) Rink Isbrae, (UI) Upernavik Isstrøm (Central), (KO) Kong Oscar Gletsjer, (PG) Petermann Gletsjer, (K) Kangerlussuaq. Scatter points are colour-coded in greyscale by the percentage of summer (JJA) days over which ice velocities were measured in that particular year (see Methods/Supplementary Information). At each site, only points common to every annual velocity field included in the time series were used for velocity extraction (see Supplementary Figs S9–S15). The dashed line displays the average velocity between 1990 and 1999, and the dotted line displays the average velocity between 2014 and 2018. Input parameters are given in Table S1.

and others, 2018, 2019) from 1985 to 2018 at tidewater glacier margins (Fig. 2) alongside these studies, we observe that those sites where ice velocities were greater between 2014 and 2018 than during the 1990s have also undergone large and/or rapid perturbations downstream. Conversely, five of the six sites without inland acceleration also exhibit acceleration downstream (Fig. 3).

Where multiple GPS sites are present upstream of an individual glacier terminus, inland change is largely consistent across these GPS sites (Fig. 1). At Kangerlussuaq however, the response is more complex. While the glacier terminus underwent a substantial acceleration between 2000 and 2006 (Rignot and Kanagaratnam, 2006; Howat and others, 2007, 2008; Bevan and others, 2012; Moon and others, 2012; Khan and others, 2014), flow diverges into four distinct branches inland (Fig. 4), with acceleration inland of the central flow branches (2 and 3) and deceleration inland of the most southerly branch (1) between 1993–1997 and 2014–2018. For the flow branches (2 and 3) where we observe inland acceleration (of 3.2 ± 1.0 to $6.5 \pm 1.4 \text{ m a}^{-1}$ and 1.7 ± 0.8 to $7.5 \pm 2.2 \text{ m a}^{-1}$ respectively, Fig. 1), we observe downstream speed-ups of $\sim 100 \text{ m a}^{-1}$ ($\sim 25\%$) and 75 m a^{-1} ($\sim 20\%$) between ~ 2000 and ~ 2008 . A similar $\sim 100 \text{ m a}^{-1}$ acceleration is observed at the most easterly branch (4), although the GPS sites inland of this flow branch are filtered out of our analysis. For the most southerly flow branch (1), inland of which we observe a deceleration ($-4.0 \pm 1.9 \text{ m a}^{-1}$, Fig. 1), we observe minimal downstream change, indicating that differences

in downstream flow dynamics may explain the different inland responses of upstream tributaries at Kangerlussuaq.

3.3 Influence of ice geometry

While glaciers that show interior acceleration are characterised by downstream acceleration, several glaciers that have also experienced downstream speed-up exhibit no inland acceleration. Consequently, dynamical change at the margin alone is not necessarily indicative of interior acceleration. To assess whether downstream ice geometry can explain the inland heterogeneity in velocity change between 1993–1997 and 2014–2018, we compare the observed velocity change to basal topography and the extent of subglacial troughs (Fig. 5, Table 1). It is clear that for six out of the eight glaciers where we observe inland acceleration, the overdeepened subglacial trough extends further or at least a comparable distance inland to the PARCA GPS stations (Table 1). This is most evident at Jakobshavn Isbrae, where we observe inland acceleration at four GPS sites, all of which lie within an extensive region underlain by deep basal topography (Fig. 5). Conversely, for four of the seven glaciers where we observe inland deceleration, the GPS stations are largely located far beyond the maximum extent of any subglacial trough, indicating that subglacial topography (and thus ice geometry) may play an important role limiting the propagation distance of perturbations at the terminus for certain glaciers. This pattern, however, is not

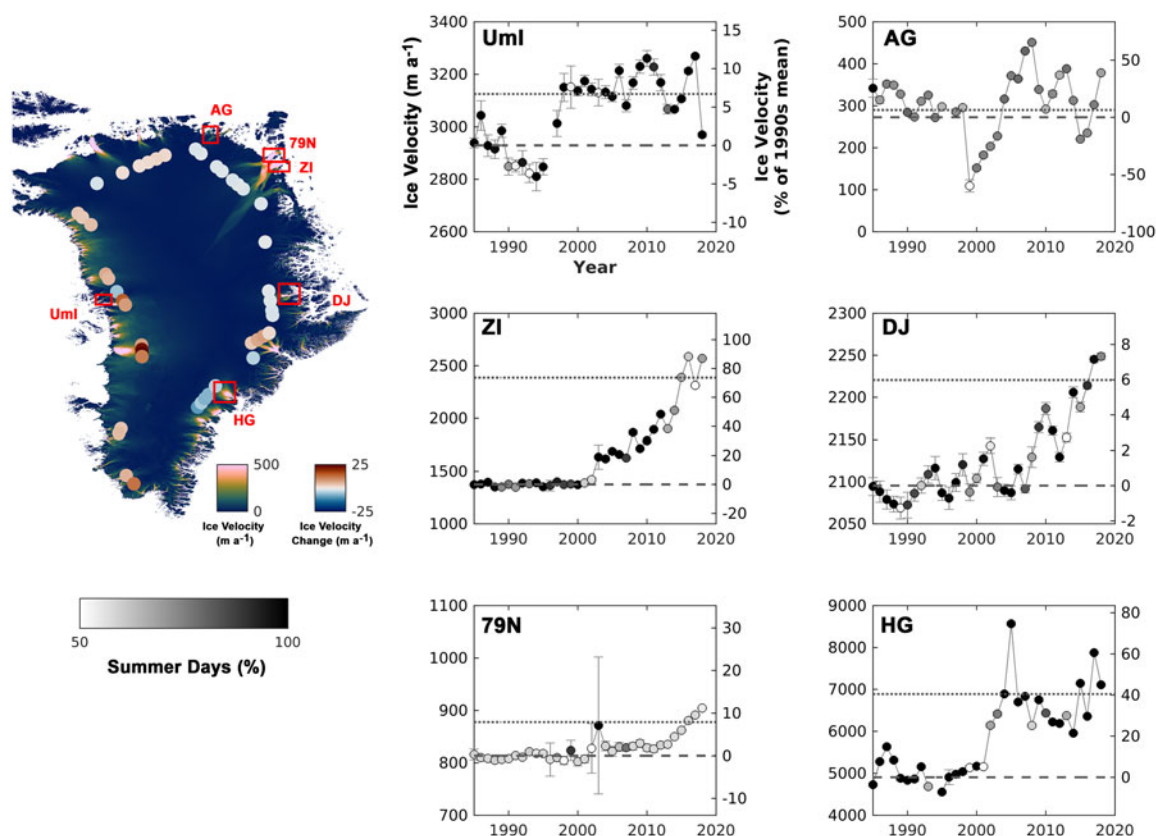


Fig. 3. Time series of ITS-LIVE ice velocity (m a^{-1}) from 1985 to 2018 measured near the terminus (see Supplementary Figs S17–S22 for exact locations) for glaciers inland of which no multi-decadal acceleration is observed; (Umi) Umiammakku Isbrae, (AG) Academy Gletsjer, (79N) 79 North Glacier, (ZI) Zachariae Isstrøm, (DJ) Dugaard-Jensen Gletsjer, (HG) Helheim Gletsjer. Scatter points are colour-coded in greyscale by the percentage of summer days over which ice velocities were measured for that particular year (see Methods/Supplementary Information). At each site, only the points common to every velocity field included in the time series were used for velocity extraction (see Supplementary Figs S16–S21). The dashed line displays the average velocity between 1990 and 1999, and the dotted line displays the average velocity between 2014 and 2018. Input parameters are given in Table S1.

ubiquitous; for example, we do not observe inland acceleration at 79 North Glacier or Zachariae Isstrøm despite extensive subglacial troughs while conversely, we observe acceleration inland of Kangerlussuaq despite the GPS sites being located ~ 50 km further inland than the head of the respective subglacial trough.

3.4 Influence of surface mass balance

Within the accumulation zone in southwest Greenland, increases in surface melt have been hypothesised to drive acceleration through hydro-dynamic coupling (Doyle and others, 2014) and/or cryo-hydrologic warming (Phillips and others, 2010, 2013). Data from MAR v3.10 (Fettweis and others, 2017) suggest ice-sheet-wide increases in modelled surface melt production within the interior (Figs 6a, b) between the periods 1990–1999 and 2014–2018. The largest increases ($42\text{--}270 \text{ mm a}^{-1}$) are observed in the west and southeast, whereas increases in the north and northeast are very small ($0\text{--}45 \text{ mm a}^{-1}$). All of the PARCA GPS sites are characterised by positive SMBs during both the 1990–1999 and 2014–2018 periods (Figs 6c, d), which range from $\sim 90\text{--}200 \text{ mm a}^{-1}$ in the north to more positive values of $\sim 200\text{--}1900$ and $\sim 300\text{--}650 \text{ mm a}^{-1}$ along the east and west coasts, respectively.

4. Discussion

4.1. Mechanisms driving inland change

Our results reveal a complex pattern of inland velocity change over the ~ 20 -year period between 1993–1997 and 2014–2018, for which there exist several possible driving mechanisms.

While we do observe increases in modelled surface melt production at all of the GPS sites, and decreases in modelled SMB at most (Fig. 6), we see no evidence that any of the sites have undergone a transition from the accumulation to the ablation zone during the study period. Although cryo-hydrologic warming may also occur in the wet snow zone of the lower accumulation zone (Phillips and others, 2013), all 45 sites remain well within the accumulation zone as evidenced by positive modelled SMBs during 2014–2018 (all $> \sim 10 \text{ cm w.e.}$, with a mean of 43 cm w.e. , Fig. 6d). This is consistent with in situ stake observations which show no evidence of negative SMB above $\sim 1700 \text{ m (a.s.l.)}$ across 17 sites in Greenland (Machguth and others, 2016), and a persistent positive SMB at site S10 (1850 m a.s.l.) of the K-transect in southwest Greenland (van de Wal and others, 2012), despite increases in surface melt at this site (Doyle and others, 2014). Furthermore, analysis of surface strain rates indicates that moulins and crevasses are unlikely to form above 1600 m (a.s.l.) , and so meltwater access to the englacial drainage system is likely limited at these elevations (Poinar and others, 2015) and will instead flow along surface streams into moulins further downstream.

Ice flow may also be affected by the presence of firn aquifers, which are thought to be extensive in southeast Greenland (Miege and others, 2016; Brangers and others, 2020) and which may store significant quantities of meltwater for several decades (Harper and others, 2012; Forster and others, 2014; Miller and others, 2018). Water stored in firn may increase ice motion through latent heat transfer (Phillips and others, 2010, 2013; Poinar and others, 2017) and/or through drainage to the bed (Miege and others, 2016; Poinar and others, 2017, 2019). In the case of the

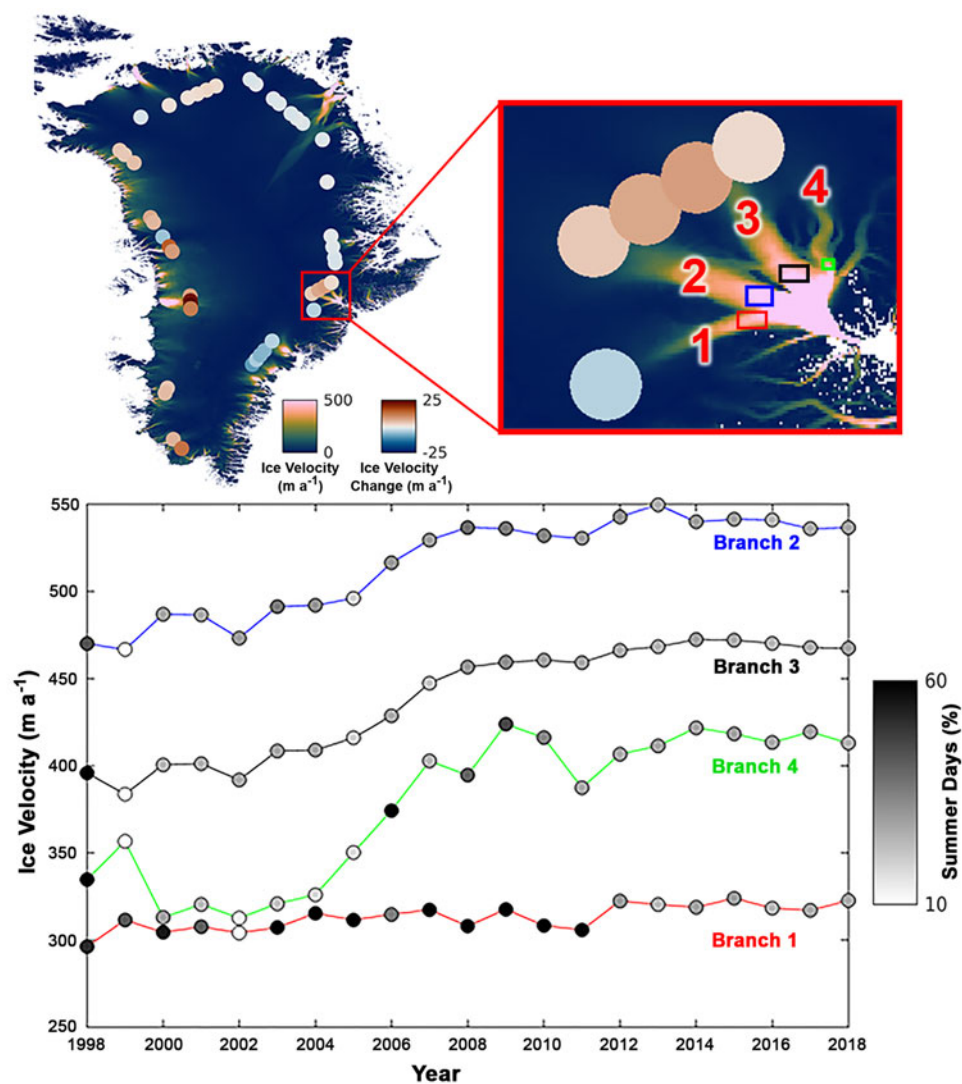


Fig. 4. Time series of ITS-LIVE ice velocity (m a^{-1}) from 1998 to 2018 measured at the four flow branches of Kangerlussuaq, with velocity extraction from pixels within the rectangle on each branch. Scatter points are colour-coded by the percentage of summer days over which ice velocities were measured for that particular year (see Methods/Supplementary Information). At each site, only the points common to every velocity field included in the time series were used for velocity extraction (see SI Figs S22–S25). Input parameters are given in Table S1.

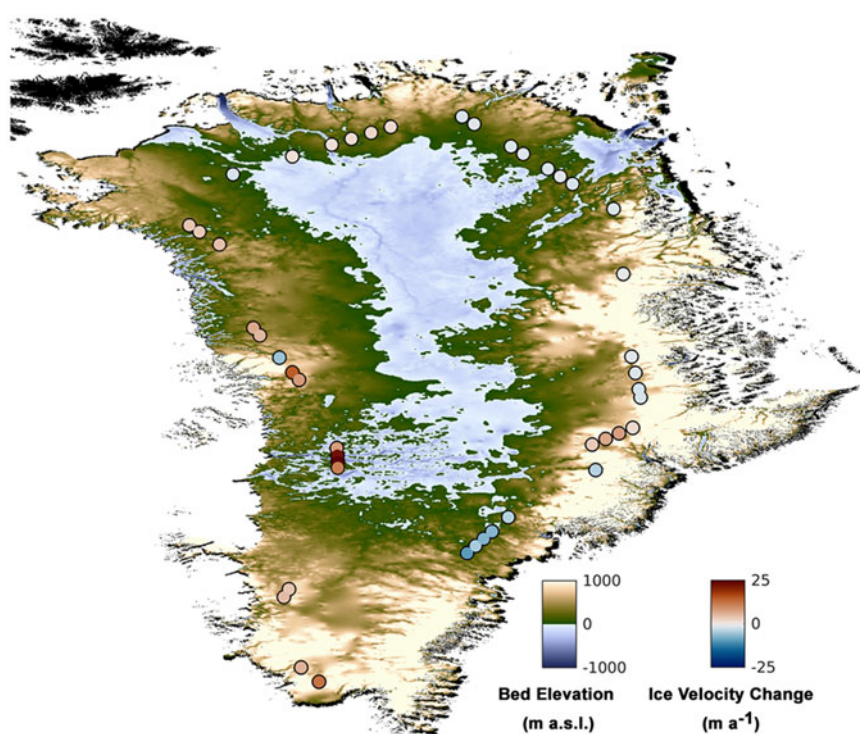


Fig. 5. Ice velocity change (m a^{-1}) at 45 GPS sites inland of tidewater margins between the periods 1993–1997 and 2014–2018, compared to basal topography from BedMachineV3 (Mortlighem and others, 2017).

Table 1. Comparison of PARCA GPS distance inland and measured velocity change (m a^{-1}) between 1993–1997 and 2014–2018 with the extent of subglacial troughs (Morlighem and others, 2014, Table S1) at 15 tidewater glaciers on the Greenland Ice Sheet

	Distance of PARCA GPS site from terminus (km)				Inland velocity change (m a ^{−1})	
Glacier name Location	Min	Max	Subglacial trough length (km) ^a (Morlighem and others, 2014)	Trough length – average distance inland (km)	Min	Max
Central and southwest						
Narsap Sermia	92	92	77	−15	3.6	4.6
Jakobshavn Isbrae	117	118	170	52.5	7.6	28.1
Northwest						
Rink Isbrae	90	94	88	−4	7.8	14.6
Umiammakku Isbrae	115	115	39	−76	−5.5	−5.5
Upernavik Isstrøm (C)	97	97	90	−7	4.9	6.3
Kong Oscar Gletsjer	85	86	101	15.5	3.3	3.7
North						
Petermann Gletsjer	200	200	400	200	1.1	1.1
Ryder Gletsjer	180	216	191	−7	1	2.1
Academy Gletsjer	153	165	102	−57	−1.8	−1.3
Northeast						
79 North Glacier	210	219	404	189.5	−1.6	−1.5
Zachariae Isstrøm	190	240	377	162	−1.8	−1.3
Central and southeast						
Daugaard-Jensen Gletsjer	108	137	70 ^b	−52.5	−1.5	−1.3
Kangerlussuaq	131	141	87	−49	−4	7.5
Helheim Gletsjer	118	120	68	−51	−6.8	−4.1
Ikertivaq	96	130	0	−113	−9.4	−4.9

As neighbouring GPS sites may have differing distances from the margin, we compare the average distance of these sites inland of a particular glacier to the subglacial trough length at that glacier.

^aSubglacial trough lengths were calculated by Morlighem and others (2014, Table S1) using the longest flowline that connects the ice front to the interior of the ice sheet, and do not necessarily follow the glacier centreline.

^bDaugaard-Jensen Gletsjer is stated to have a trough length of 70 km in the main manuscript, with a maximum trough length of 124 km given in Supplementary Information.

latter, the presence of a firm aquifer may buffer the supply of meltwater to the bed, and thus possibly mask any long-term trend between ice velocity and meltwater production. However, drainage from firm aquifers is thought to most likely occur where there exists a downstream crevasse field through which it can drain to the bed (Miège and others, 2016), and so may have a limited impact upon ice flow at the inland locations assessed in this study.

Changes in surface slope and/or ice thickness through both ice dynamical and SMB-related processes cause changes in driving stress and can thus contribute to changes in ice motion through changes to the internal deformation rate. To assess whether the velocity changes observed may be explained by changes in local driving stress, we estimate the expected change in velocity as a result of changes in ice thickness and surface slope at PARCA GPS site 36, inland of Jakobshavn Isbrae, where we observe the largest velocity increase. Applying this calculation elsewhere is difficult as the observed velocity changes are small (Fig. 1), the uncertainties associated with the SEC are proportionally large, and the potential errors associated with the following 20-year approximate SEC reconstruction, and thus the 1990s slope estimate, are too great, thus reducing confidence in our ability to make any meaningful comparison.

We extract ice thickness and surface slope, the latter calculated using surface elevation and under the assumption that ice flows in the direction of the steepest slope, at this location from BedMachineV3 (Morlighem and others, 2017), and consider this as a representative for the period 2014–2018. We then use the CCI SEC v2.0 product (Simonsen and Sørensen, 2017; Sørensen and others, 2018) to calculate the cumulative SEC at each pixel within the 3×3 -pixel window surrounding site 36, across the periods 1993–1997, 1998–2002, 2003–2007, 2007–2011 and 2012–2016. By adding this SEC to the ice thickness from BedMachineV3, we get a rough estimate of the initial ice thickness in 1993. Similarly, by adding the cumulative SEC to the BedMachineV3 surface elevation within the same 3×3 -pixel window, we calculate an approximate initial surface slope for 1993. We subsequently calculate the change in ice thickness and surface slope.

The first-order relative change in surface velocity (δu_s) as a result of changes in ice thickness and surface slope can be characterised by the following (Tedstone and others, 2015):

$$\delta u_s = u_s \left(3 \frac{\delta S}{S} + 4 \frac{\delta H}{H} \right)$$

where u_s represents the initial ice surface velocity (194.5 m a^{-1}), S and H represent the initial surface slope (0.018 m m^{-1}) and ice thickness (1740.2 m), respectively, and δS and δH represent the change in surface slope (0.001 m m^{-1}) and ice thickness (-7.2 m), respectively. The resultant approximation for a change in deformational velocity is 35.02 m a^{-1} , which is within the uncertainty range of the observed velocity change ($28.1 \pm 7.8 \text{ m a}^{-1}$) and thus compares well.

We also assess the role that SMB-driven thickness changes play in driving velocity change (Mernild and others, 2013). There has been extensive SMB-driven thinning around Greenland (van den Broeke and others, 2009; Mouginot and others, 2019), for example, at site 36, modelled melt production increases by 150 mm a^{-1} between the 1990–1999 and 2014–2018 means (Fig. 6a). However, we observe no obvious spatial correlation between changes in ice velocity (Fig. 1) and modelled surface melt production. While we do observe large increases in surface melting ($>100 \text{ mm a}^{-1}$) at some GPS sites where we observe acceleration (i.e. inland of Jakobshavn Isbrae, Upernavik Isstrøm and Kong Oscar Gletsjer in the central to northwest), the GPS sites on the east coast show an almost pervasive deceleration despite increases in modelled melt production. This is most notable at the south-eastern GPS sites, where increases in modelled melt production are of a similar or greater magnitude (47 – 270 mm a^{-1}) to those in the central and northwest (42 – 162 mm a^{-1}).

To assess the impact of this SMB forcing alone, we follow Tedstone and others (2015) by taking a 100 km transect, extending 50 km on either side of site 36, and calculating the slope change from the linear change in ice thickness over this distance.

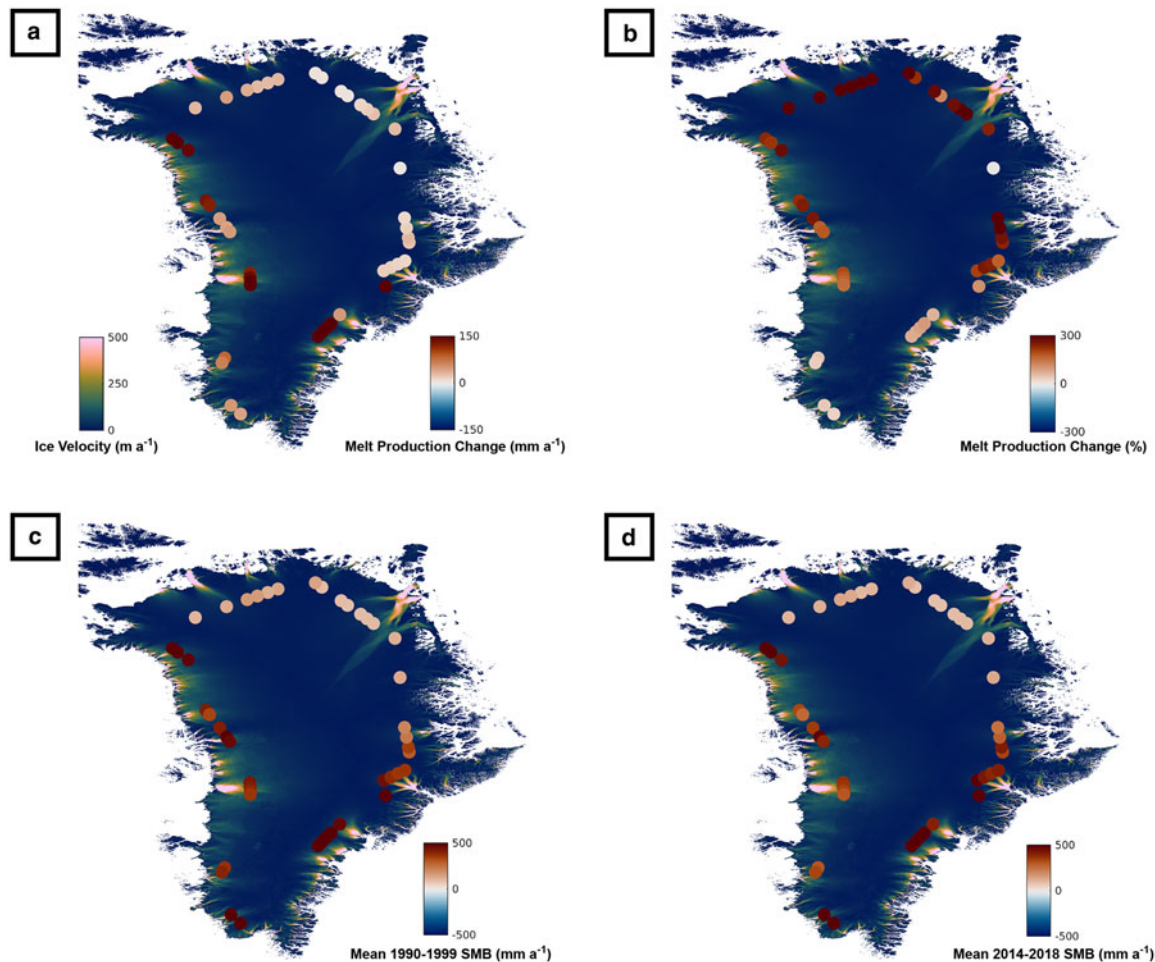


Fig. 6. (a) Modelled surface melt production change (mm a^{-1}), (b) modelled surface melt production change (%), (c) mean modelled 1990–1999 SMB (mm a^{-1}) and (d) mean modelled 2014–2018 SMB (mm a^{-1}) at 45 GPS sites inland of tidewater margins. Modelled melt production change is calculated between the 1990–1999 and 2014–2018 means. The base image is the 2016 velocity field from the NASA MEaSUREs ITS-LIVE v0 product (Gardner and others, 2018, 2019). Modelled surface melt production and SMB data are from MAR v3.10 (Fettweis and others, 2017).

Modelled melt production increased by 184.5 and 41.3 mm a^{-1} between the 1990–1999 and 2014–2018 means at the downstream and upstream ends of the transect, respectively, a difference of 143.2 mm a^{-1} , and the concurrent change in accumulation rate is negligible. Assuming a linear increase in melt production over 20 years, this gives a total thinning of 1.5 m and a steepening of $0.000015 \text{ m m}^{-1}$.

Applying the above equation, we estimate the associated change in deformational velocity as -0.18 m a^{-1} , indicating that at site 36, SMB changes alone are unable to explain the observed velocity acceleration, and counteract some of the observed velocity increase. The modelling therefore suggests that in this inland region of the ice sheet, changes in surface slope are insufficient to overcome the reduction in driving stress caused by thinning. At all other sites where we observe acceleration, modelled melt production increase is either similar (northwest Greenland) or less than that observed inland of Jakobshavn Isbrae (Fig. 6a). As such, assuming a relatively consistent ice-sheet hypsometry, this suggests that a change in SMB may often act to oppose acceleration and is unlikely to drive an inland velocity change of more than several tens of cm a^{-1} .

Changes to SMB have also been hypothesised to influence ice motion through cryo-hydrologic warming in regions transitioning from the accumulation to the ablation region (Phillips and others, 2010, 2013). Despite increases in modelled melt production, we observe that all of the PARCA GPS sites have strongly positive modelled SMB in both the 1990–1999 and 2014–2018 periods

(Figs 6c, d), and so we observe no evidence of a transition between accumulation and ablation zones at any site, with all 45 GPS sites remaining well within the accumulation zone.

As a result, we argue that our observations of inland acceleration are most likely driven by the upstream propagation of changes initiated at the terminus (Howat and others, 2005, 2007; Joughin and others, 2008; Price and others, 2008, 2011; Nick and others, 2009; Felikson and others, 2017). This mechanism is discussed in more detail in the subsequent sections.

4.2. Observed velocity changes and regional differences

We observe almost ubiquitous acceleration across the GPS sites inland of tidewater glaciers in west Greenland with a slowdown at Umiammakku Isbrae being the only exception. The largest acceleration is observed $\sim 117 \text{ km}$ inland from the terminus of Jakobshavn Isbrae (7.6 ± 4.2 to $28.1 \pm 7.8 \text{ m a}^{-1}$), which is unsurprising given the high magnitude of acceleration and thinning observed near the terminus between the late-1990s and early-2010s (Joughin and others, 2004, 2008, 2014, 2018; Luckman and Murray, 2005; Holland and others, 2008; Moon and others, 2012), primarily as a result of reduced back-stress through the loss of its floating ice tongue (Joughin and others, 2004; Thomas, 2004; Holland and others, 2008; Motyka and others, 2011). Moreover, modelling of dynamic thinning suggests that faster ice flow facilitates a larger magnitude propagation inland, with modelled thinning rates at 2000 m elevation of nearly

-0.4 m a^{-1} within a drainage system with a mean flow velocity of $\sim 120 \text{ m a}^{-1}$ as opposed to an ice-sheet-wide average of $\sim -0.1 \text{ m a}^{-1}$ with a mean velocity of $\sim 60 \text{ m a}^{-1}$ (Wang and others, 2012), and Jakobshavn Isbrae is the fastest flowing outlet glacier on the GrIS (i.e. Joughin and others, 2014, 2018).

We also observe inland acceleration at other tidewater glaciers in west Greenland that have undergone terminus retreat and associated near-terminus acceleration, such that their 2014–2018 ice velocities were greater than during the 1990s (Fig. 2). For example, the northern and central branches of Upernavik Isstrøm underwent rapid calving, retreat and acceleration beginning during the mid-late 2000s (Khan and others, 2013; Larsen and others, 2016), and Narsap Sermia accelerated and retreated by $\sim 3.3 \text{ km}$ between 2010 and 2014, primarily as a result of increased submarine melting (Motyka and others, 2017). Similarly, Kong Oscar Gletsjer and Rink Isbrae retreated by several kilometres during the mid-2000s (Bevan and others, 2012) and the mid-late 1990s (Catania and others, 2018) respectively, in conjunction with acceleration (Fig. 2). Inland of these west coast glaciers, we observe acceleration ranging from 3.3 ± 1.0 to $3.7 \pm 2.4 \text{ m a}^{-1}$ inland of Kong Oscar Gletsjer up to $14.6 \pm 7.5 \text{ m a}^{-1}$ inland of Rink Isbrae. However, we observe a clear contrast between the dynamics of west and east Greenland. While outlet glaciers on the west coast almost all demonstrate inland acceleration, there is little evidence of propagation of downstream change inland of tidewater glacier termini on the east coast. We observe no evidence of inland acceleration at Helheim Gletsjer, Zachariae Isstrøm and 79 North Glacier, all of which have undergone significant frontal retreat and acceleration at some point between our measurement periods of 1993–1997 and 2014–2018 (Howat and others, 2005, 2007, 2008; Rignot and Kanagaratnam, 2006; Murray and others, 2010; Bevan and others, 2012; Mouginot and others, 2015; our Fig. 3).

The duration of a specific terminus perturbation does not appear to control the likelihood of that perturbation propagating inland. We observe inland acceleration at sites with long-term perturbations (Jakobshavn Isbrae, Upernavik Isstrøm, Kong Oscar Gletsjer) as well as at sites with relatively short-term accelerations (i.e. Kangerlussuaq, Narsap Sermia), although all sites where we observe acceleration were flowing faster in their terminus regions during 2014–2018 than during 1990–1999. Moreover, we observe no inland acceleration at Zachariae Isstrøm despite continual acceleration since the early-2000s, or at Helheim Gletsjer which underwent a rapid speed-up of short duration from ~ 2002 to 2005 (Fig. 3). It may be that perturbations at the terminus have yet to propagate to the PARCA GPS sites inland of some tidewater glaciers, particularly in the north and northeast (Fig. S6) where the GPS sites are ~ 165 – 240 km inland from the terminus as opposed to ~ 85 – 141 km on the east and west coasts. Thinning has been observed to propagate along ice streams in West Antarctica at the rates of 6 – 15 km a^{-1} (Konrad and others, 2017) while acceleration near the terminus of Kangerlussuaq propagated 10 km up-glacier between 2005 and 2006 (Howat and others, 2007). While recent work observes propagation rates in the lowest 20 km of Jakobshavn Isbrae an order of magnitude faster than the local mean flow speed (Riel and others, 2020), the rates of propagation have not been observed further inland, or elsewhere in Greenland, and we are unable to determine propagation rates given the gap in our time series. Surface velocities derived from Landsat missions prior to Landsat-8 are characterised by both a reduced spatial coverage in inland regions, due to insufficient radiometric resolution to measure subtle features on the ice-sheet surface (Fahnestock and others, 2016), and increased uncertainties, which are particularly problematic given the slow surface velocities as one moves inland. Regardless, it is plausible that

perturbations have not yet had the time to propagate sufficiently far inland to be observed at the PARCA GPS sites in northeast Greenland, especially given that the rate of propagation will slow as it moves further inland (van der Veen, 2001). This is supported by separate velocity measurements, which show no evidence of acceleration beyond ~ 80 – 100 and $\sim 50 \text{ km}$ inland of Zachariae Isstrøm and 79 North Glacier, respectively (Mouginot and others, 2015; their Fig. 2). Further south at Dagaard-Jensen and Helheim Gletsjers however, the PARCA GPS sites are a comparable distance inland to those on the west coast, as well as those at Kangerlussuaq, which have undergone acceleration in response to terminus perturbations, indicating that there may be an alternative control on the speed and/or limit of propagation (i.e. Felikson and others, 2017, 2020).

4.3. Influence of basal topography and ice geometry

Basal topography is a crucial factor controlling ice flow. Beneath the GrIS, widespread ice-filled valleys have been observed to extend significantly deeper below sea level and farther inland than previously thought (Morlighem and others, 2014), thereby channelling ice flow over distances from tens to hundreds of kilometres. Since deep troughs and the associated thicker ice lead to both higher driving stresses and warmer ice, they will encourage faster ice flow and potentially greater propagation distances (Wang and others, 2012). We observe almost ubiquitous interior acceleration in the central and northwest regions, across areas that are characterised by low surface slopes and bed topography that remains below sea level for tens to hundreds of kilometres inland (Morlighem and others, 2017).

For example, Jakobshavn Isbrae flows through a subglacial valley extending $\sim 170 \text{ km}$ inland (Morlighem and others, 2014), whereas the PARCA GPS sites are located $\sim 117 \text{ km}$ from the terminus (Table 1). Under these conditions, not only do we observe the large acceleration at the terminus, but this acceleration is likely to be channelled to, and beyond, the site at which we measure inland velocity change in this study. Similar patterns are observed at other west coast glaciers, where PARCA GPS sites are closer to the margin than the extent of the associated subglacial valleys, or, if further inland than the head of the valley, are at least within the theoretical stress-coupling length (4 – $10 \times$ the ice-thickness (Kamb and Echelmeyer, 1986)) of the maximum subglacial valley extent. In contrast, the one glacier on the west coast where we do not observe inland acceleration is Umiarmakku Isbrae, despite near-terminus flow velocities $\sim 200 \text{ m a}^{-1}$ greater in the 2000s and 2010s compared to the early- to mid-1990s (Fig. 3). Here, an over-deepened subglacial valley extends just $\sim 39 \text{ km}$ from the terminus (Morlighem and others, 2014), whereas the PARCA GPS site is located $\sim 115 \text{ km}$ inland.

In the north, we observe no inland acceleration at Academy Gletsjer, where the head of the submarine valley is $\sim 57 \text{ km}$ closer to the terminus than the PARCA GPS sites. Similarly, outside of two flow branches of Kangerlussuaq, we observe no evidence of interior propagation on the east coast, where despite the existence of deep subglacial valleys (Morlighem and others, 2017), basal topography rises quickly to plateaus above sea level (Morlighem and others, 2014), suggesting that these rapid rises in basal topography may limit the inland propagation of any thinning perturbation. This is the case at Helheim Gletsjer and Dagaard-Jensen Gletsjer, which are both grounded below sea-level for $\sim 70 \text{ km}$, whereupon rises in basal topography over a short-distance have been theorised to prevent rapid glacier retreat or ice-sheet draw-down (Morlighem and others, 2014). Given that the PARCA GPS sites inland of Helheim Gletsjer and Dagaard-Jensen Gletsjer are ~ 118 – 120 and 108 – 137 km from the terminus, respectively, it is plausible that any perturbation at the terminus is limited

by the rapid rise in basal topography at the end of the subglacial trough, such that no inland response is observed in our study.

This hypothesis, and our observations, is largely consistent with recent work that argues that steep rises (termed 'knick-points') in bedrock topography act to limit the extent of inland thinning, such that the gentle basal topography of the northwest facilitates the propagation of thinning far into the ice-sheet interior, and the mountainous basal topography of the central east and southeast limits propagation to near the margin (Felixson and others, 2020). We observe inland acceleration at Rink Isbrae, Upernavik Isstrøm and Kong Oscar Gletsjer in the northwest, consistent with proposed thinning limits of >400, >300 and ~500 km, respectively (Felixson and others, 2020). Likewise, our observation of no inland speed-up at Umiammakku Isbrae is consistent with a thinning limit of 43.8 km, considerably downstream of the PARCA GPS site. Our results are also in agreement on the east coast, where Daugaard-Jensen Gletsjer and Helheim Gletsjer are characterised by thinning limits of 53.5 and 26.7 km (Felixson and others, 2020), again located >50 km downstream of the PARCA GPS sites and in line with the lack of inland acceleration observed in this study. While both 79 North and Zachariae Isstrøm show no inland acceleration despite extensive subglacial valleys extending beyond the PARCA GPS sites, as noted previously, it is plausible that since these sites are several hundred kilometres from the margin, the propagation speed is such that any downstream perturbation has not yet reached them. Alternatively, knickpoints in bed topography may limit any dynamic propagation to ~100–120 km inland of the termini of these glaciers, considerably downstream from the PARCA GPS sites in this region (Felixson and others, 2020).

Our observations of inland acceleration at Jakobshavn Isbrae, Narsap Sermia and Kangerlussuaq, however, are in contrast to the thinning limits suggested by Felixson and others (2020) at these glaciers (57.9, 37.3 and 35.3 km, respectively). Since Felixson and others (2020) argue that the $Pe = 3$ threshold accounts for 89% (with an interquartile range of 76–100%) of the total dynamic loss, our observations of acceleration inland of these glaciers may represent the remaining ~11% of dynamic change that has propagated beyond the empirical thinning limit. Alternatively, at Jakobshavn Isbrae, there may be some uncertainty associated with the choice of flowline within the Pe analysis, with earlier work indicating a thinning limit of 240 km (Felixson and others, 2017) compared to the more recent 57.9 km estimate (Felixson and others, 2020).

While we observe acceleration inland of the suggested thinning limits at Jakobshavn Isbrae and Narsap Sermia, these accelerations remain consistent with the extent of underlying subglacial troughs (Table 1). In contrast, at Kangerlussuaq, our observed acceleration is both ~100 km inland of the thinning limit proposed by Felixson and others (2020), and ~49 km inland of the maximum subglacial trough extent. Consequently, while basal topography and ice geometry appear to offer a compelling explanation for much of the observed inland velocity change, it is clear that the processes controlling tidewater glacier dynamics are complex. As such, multiple controls will likely impact the ability of a terminus perturbation to propagate inland, thus affecting how different inland regions of the GrIS have responded and will continue to respond to climate warming.

4.4. Comparison with other studies

Recent measurements of mass change between 2003 and 2019 from ICESat and ICESat-2 show a clear pattern of coastal thinning around the entire periphery of the GrIS, which decreases inland and changes to thickening at 2000–2500 m (a.s.l.) in southern and western Greenland, and at 1500 m (a.s.l.) in the northeast (Smith and others, 2020). Thinning extends furthest inland at

Jakobshavn Isbrae and in the northwest, consistent with our observations of multi-decadal accelerations in these inland regions. Similarly, mass change is far more limited in extent in the central east and northeast regions where we do not observe inland acceleration, although in the southeast, thinning appears to extend to approximately the locations of the GPS sites at which we observe no acceleration. As the dynamic component of mass change is not isolated in these ICESat and ICESat-2 data, the south-eastern thinning may be influenced by a decrease in SMB, which has contributed to $36 \pm 12\%$ of mass loss in this region between 1972 and 2018 (Mouginot and others, 2019).

Measurements of SEC can be used to isolate the dynamic component of a thinning signal through the differencing of measured elevation change and modelled SMB (i.e. Pritchard and others, 2009; McMillan and others, 2016). This methodology has revealed extensive dynamic thinning, penetrating deep into the ice-sheet interior. At Jakobshavn Isbrae, thinning has been observed ~120 km inland (Pritchard and others, 2009), extending upwards of 2000 m surface elevation as early as 2001 (Thomas and others, 2003). Similar pervasive thinning has been observed inland of other fast-flowing tidewater glaciers, notably Helheim Gletsjer, Kangerlussuaq, Upernavik Isstrøm and Zachariae Isstrøm (Pritchard and others, 2009; McMillan and others, 2016). On a regional scale, the northwest and southeast margins are characterised by the strongest dynamic thinning (Pritchard and others, 2009; Zwally and others, 2011; Csatho and others, 2014) although the furthest propagation of thinning inland is observed in the west and northwest, with thinning in the southeast less extensive (Zwally and others, 2011; Csatho and others, 2014). Moreover, in the southeast, the inland extent of dynamic thinning has been observed to rapidly decrease between the period 2003–2005 and 2009 (Csatho and others, 2014), and outside of Kangerlussuaq, significant signals of dynamic thinning are not clear (McMillan and others, 2016).

These observations are reinforced by modelling work, which indicates that dynamic thinning may penetrate deep into the ice sheet in as little as 10 years of an initial perturbation, with modelled thinning rates of up to 40 cm a^{-1} extending to 2000 m elevation in central west and northwest Greenland (Wang and others, 2012). For the fast-flowing outlet glaciers of Jakobshavn Isbrae, Helheim Gletsjer and Kangerlussuaq, modelling of dynamic thinning along the centre-profile between 2003 and 2005 suggests thinning during this period would reach ~80–100 km inland of the terminus at Jakobshavn Isbrae and ~30–40 km inland at both Helheim Gletsjer and Kangerlussuaq (Price and others, 2011).

Our work largely supports these studies. We observe a strong interior acceleration inland of Jakobshavn Isbrae, a region characterised by extremely strong dynamic thinning (Pritchard and others, 2009; Zwally and others, 2011; Csatho and others, 2014; McMillan and others, 2016), with speed-ups of smaller magnitude inland of other west coast tidewater glaciers. We observe interior acceleration upstream of two of the main flow branches of Kangerlussuaq on the east coast, and do not measure any long-term interior acceleration inland of Helheim Gletsjer or Zachariae Isstrøm, despite indications of some penetration of dynamic thinning inland at these glaciers (Pritchard and others, 2009; McMillan and others, 2016). Our observations in northeast Greenland are supported by other satellite-image-derived velocities, which indicate little if any interior acceleration inland of Zachariae Isstrøm and 79 North Glacier beyond ~80–100 and ~50 km from the terminus, respectively (Mouginot and others, 2015).

5. Conclusions

In this study, we present the first multi-decadal analysis of ice-sheet-wide changes in ice velocity within the accumulation

zone of the GrIS. Along the west coast, we observe evidence of inland acceleration, most likely in response to perturbations originating at tidewater glacier termini. In contrast, away from Kangerlussuaq, we observe no inland acceleration on the east coast, despite acceleration and thinning at the terminus of many of these marine-terminating glaciers. The complexity within the observed pattern of inland change likely reflects a range of controls, including the speed at which a perturbation can propagate inland, and the influence of ice geometry and basal topography in facilitating or limiting the extent to which a perturbation can propagate up-glacier.

These findings are of great importance with regards to Greenland's future contribution to global sea-level rise, as they indicate that ice acceleration at many tidewater glaciers has the potential to propagate considerable distances into the ice-sheet interior, accelerating the draw-down of greater volumes of thicker ice towards the margins, thus accelerating mass loss. Moreover, our results indicate that this mass loss as a result of the draw-down of ice from the interior should be further exacerbated by future acceleration and thinning perturbations at tidewater margins. However, our results also support recent work that indicates that local ice geometry and bed topography are crucial in facilitating or limiting the ability for a perturbation at the terminus to propagate inland (Morlighem and others, 2014, 2017; Felikson and others, 2017, 2020), and suggest that as a result of steep down-glacier bed topography, inland regions in east Greenland may be more resilient to the impacts of future outlet glacier acceleration than those in the west. This is consistent with recent work that suggests that the presence of steep subglacial knickpoints limits the extent to which thinning can diffuse inland, particularly in the southeast, whereas the gentle bed topography of the northwest facilitates the propagation of thinning hundreds of kilometres inland (Felikson and others, 2020). Consequently, we expect that Greenland's future contribution to global sea-level rise will be spatially complex and will depend on the ability for dynamic changes at the termini of individual outlet glaciers to propagate inland.

Supplementary material. The supplementary material for this article can be found at <https://doi.org/10.1017/jog.2021.31>

Acknowledgements. J.J.W. was funded by a UK Natural Environment Research Council (NERC) doctoral training partnership grant (NE/L002558/1). We thank Xavier Fettweis for providing the MAR v3.10 SMB data, and Denis Felikson for helpful discussions with regards to the propagation of terminus perturbations inland. We also thank the two reviewers whose suggestions and comments helped improve the manuscript.

Author contributions.

J.J.W., N.G. and P.N. contributed to the design of the study and the writing of the paper. J.J.W. performed data processing and analyses.

References

- Ahlström AP and 13 others (2013) Seasonal velocities of eight major marine-terminating outlet glaciers of the Greenland ice sheet from continuous in situ GPS instruments. *Earth System Science Data* **5**(2), 277–287.
- Bamber JL, Westaway RM, Marzeion B and Wouters B (2018) The land ice contribution to sea level during the satellite era. *Environmental Research Letters* **13**(6), 099502.
- Bartholomew I and 5 others (2010) Seasonal evolution of subglacial drainage and acceleration in a Greenland outlet glacier. *Nature Geoscience* **3**(6), 408–411.
- Bartholomew ID and 6 others (2011) Seasonal variations in Greenland Ice Sheet motion: inland extent and behaviour at high elevations. *Earth and Planetary Science Letters* **307**(3–4), 271–278.
- Bevan SL, Luckman AJ and Murray T (2012) Glacier dynamics over the last quarter of a century at Helheim, Kangerdlugssuaq and 14 other major Greenland outlet glaciers. *The Cryosphere* **6**, 923–937.
- Brangers I and 5 others (2020) Sentinel-1 detects firn aquifers in the Greenland Ice Sheet. *Geophysical Research Letters* **47**(3), <https://doi.org/10.1029/2019GL085192>.
- Bunce C, Carr R, Nienow PW, Ross N and Killick R (2018) Ice front change of marine-terminating outlet glaciers in northwest and southeast Greenland during the 21st century. *Journal of Glaciology* **64**(246), 523–535.
- Catania G and 7 others (2018) Geometric controls on tidewater glacier retreat in central western Greenland. *Journal of Geophysical Research: Earth Surface* **123**(1), 2024–2038.
- Csatho BM and 9 others (2014) Laser altimetry reveals complex pattern of Greenland ice sheet dynamics. *Proceedings of the National Academy of Sciences* **111**, 18478–18483.
- Cuffey KM and Paterson WSB (2010) *The Physics of Glaciers*, 4th Edn. Oxford: Butterworth-Heinemann.
- Dehecq A, Gourmelen N and Trouvé E (2015) Deriving large-scale glacier velocities from a complete satellite archive: application to the Pamir-Karakoram-Himalaya. *Remote Sensing of Environment* **162**, 55–66.
- Doyle SH and 6 others (2014) Persistent flow acceleration within the interior of the Greenland ice sheet. *Geophysical Research Letters* **41**(3), 899–905.
- Enderlin EM and 5 others (2014) An improved mass budget for the Greenland ice sheet. *Geophysical Research Letters* **41**(3), 866–872.
- Fahnestock M and 5 others (2016) Rapid large-area mapping of ice flow using Landsat 8. *Remote Sensing of Environment* **185**, 84–94.
- Felikson D and 11 others (2017) Inland thinning on the Greenland ice sheet controlled by outlet glacier geometry. *Nature Geoscience* **10**(5), 366–369.
- Felikson D, Catania G, Bartholomew TC, Morlighem M and Noël B (2020) Steep glacier bed knickpoints mitigate inland thinning in Greenland. *Geophysical Research Letters*. doi: [10.1029/2020GL090112](https://doi.org/10.1029/2020GL090112).
- Fettweis X and 8 others (2017) Reconstructions of the 1900–2015 Greenland ice sheet surface mass balance using the regional climate MAR model. *The Cryosphere* **11**(2), 1015–1033.
- Forster RR and 12 others (2014) Extensive liquid meltwater storage in firn within the Greenland ice sheet. *Nature Geoscience* **7**, 95–98.
- Gagliardini O and Werder MA (2018) Influence of increasing surface melt over decadal timescales on land-terminating Greenland-type outlet glaciers. *Journal of Glaciology* **64**(247), 700–710.
- Gardner AS and 6 others (2018) Increased West Antarctic and unchanged East Antarctic ice discharge over the last 7 years. *The Cryosphere* **12**(2), 521–547.
- Gardner AS, Fahnestock MA and Scambos TA (2019) ITS_LIVE regional glacier and ice sheet surface velocities, data archived at National Snow and Ice Data Center (data accessed 06/06/2019). doi: [10.5067/6II6VW8LLWJ7](https://doi.org/10.5067/6II6VW8LLWJ7).
- Goelzer H and 41 others (2020) The future sea-level contribution of the Greenland ice sheet: a multi-model ensemble study of ISMIP6. *The Cryosphere* **14**(9), 3071–3096.
- Hanna E and 8 others (2008) Increased runoff from melt from the Greenland Ice Sheet: a response to global warming. *Journal of Climate* **21**(2), 331–341.
- Harper J, Humphrey N, Pfeffer WT, Brown J and Fettweis X (2012) Greenland ice-sheet contribution to sea-level rise buffered by meltwater storage in firn. *Nature* **491**, 240–243.
- Hill EA, Carr R, Stokes CR and Gudmundsson H (2018) Dynamic changes in outlet glaciers in northern Greenland from 1948 to 2015. *The Cryosphere* **12**, 3243–3263.
- Holland DM, Thomas RH, de Young B, Ribergaard MH and Lyberth B (2008) Acceleration of Jakobshavn Isbrae triggered by warm subsurface ocean waters. *Nature Geoscience* **1**, 659–664.
- Howat IM, Joughin I, Fahnestock M, Smith BE and Scambos TA (2008) Synchronous retreat and acceleration of southeast Greenland outlet glaciers 2000–06 ice dynamics and coupling to climate. *Journal of Glaciology* **54**, 646–660.
- Howat IM, Joughin I and Scambos TA (2007) Rapid changes in ice discharge from Greenland outlet glaciers. *Science (New York, N.Y.)* **315**(5818), 1559–1561.
- Howat IM, Joughin I, Tulaczyk S and Gogineni S (2005) Rapid retreat and acceleration of Helheim Glacier, east Greenland. *Geophysical Research Letters* **32**, L22502. doi: [10.1029/2005GL024737](https://doi.org/10.1029/2005GL024737).
- Hvidberg CS and 10 others (2020) Surface velocity of the Northeast Greenland Ice Stream (NEGIS): assessment of interior velocities derived from satellite data by GPS. *The Cryosphere* **14**, 3487–3502.
- Joughin I and 8 others (2008) Ice-front variation and tidewater behaviour on Helheim and Kangerdlugssuaq Glaciers, Greenland. *Journal of Geophysical Research* **113**, F01004. doi: [10.1029/2007JF000837](https://doi.org/10.1029/2007JF000837).

- Joughin I, Abdalati W and Fahnestock M (2004) Large fluctuations in speed on Greenland's Jakobshavn Isbrae glacier. *Nature* **432**, 608–610.
- Joughin I, Shean DE, Smith BE and Floricioiu D (2020) A decade of variability on Jakobshavn Isbrae: ocean temperatures pace speed through influence on melange rigidity. *The Cryosphere* **14**(1), 211–227.
- Joughin I, Smith BE and Howat I (2018) Greenland Ice Mapping Project: ice flow velocity variation at sub-monthly to decadal timescales. *The Cryosphere* **12**(7), 2211–2227.
- Joughin I, Smith BE, Howat IM, Scambos T and Moon T (2010) Greenland flow variability from ice-sheet-wide velocity mapping. *Journal of Glaciology* **56**(197), 415–430.
- Joughin I, Smith BE, Shean DE and Floricioiu D (2014) Brief communication: further summer speedup of Jakobshavn Isbrae. *The Cryosphere* **8**, 209–214.
- Kamb B and Echelmeyer KA (1986) Stress-gradient coupling in glacier flow: I. Longitudinal averaging of the influence of ice thickness and surface slope. *Journal of Glaciology* **32**, 267–284.
- Khan SA and 13 others (2013) Recurring dynamically induced thinning during 1985 to 2010 on Upernavik Isstrøm, west Greenland. *Journal of Geophysical Research: Earth Surface* **118**, 11–121. doi: [10.1029/2012JF002481](https://doi.org/10.1029/2012JF002481).
- Khan SA and 12 others (2014) Sustained mass loss of the northeast Greenland ice sheet triggered by regional warming. *Nature Climate Change* **4**, 292–299.
- Khazendar A and 13 others (2019) Interruption of two decades of Jakobshavn Isbrae acceleration and thinning as regional ocean cools. *Nature Geoscience* **12**, 277–283.
- King MD and 6 others (2018) Seasonal to decadal variability in ice discharge from the Greenland Ice Sheet. *The Cryosphere* **12**, 3813–3825.
- King MD and 8 others (2020) Dynamic ice loss from the Greenland Ice Sheet driven by sustained glacier retreat. *Communications Earth & Environment* **1**, <https://doi.org/10.1038/s43247-020-0001-2>.
- Konrad H and 6 others (2017) Uneven onset and pace of ice-dynamical imbalance in the Amundsen Sea Embayment, West Antarctica. *Geophysical Research Letters* **44**(2), 910–918.
- Larsen SH and 5 others (2016) Increased mass loss and asynchronous behaviour of marine-terminating outlet glaciers at Upernavik Isstrøm, NW Greenland. *Journal of Geophysical Research: Earth Surface* **121**, 241–256. doi: [10.1002/2015JF003507](https://doi.org/10.1002/2015JF003507).
- Lemos A and 5 others (2018) Ice velocity of Jakobshavn Isbræ, Petermann Glacier, Nioghalvfjærdssjøen, and Zachariæ Isstrøm, 2015–2017, from Sentinel 1-a/b SAR imagery. *The Cryosphere* **12**(6), 2087–2097.
- Luckman A and Murray T (2005) Seasonal variation in velocity before retreat of Jakobshavn Isbrae, Greenland. *Geophysical Research Letters* **32**(8), L08501. doi: [10.1029/2005GL022519](https://doi.org/10.1029/2005GL022519).
- Luckman A, Murray T, de Lange R and Hanna E (2006) Rapid and synchronous ice-dynamic changes in east Greenland. *Geophysical Research Letters* **33**(3), L03503. doi: [10.1029/2005GL025428](https://doi.org/10.1029/2005GL025428).
- Machguth H and 9 others (2016) Greenland meltwater storage in firn limited by near-surface ice formation. *Nature Climate Change* **6**(4), 390–393.
- Mankoff KD and 5 others (2020) Greenland Ice Sheet solid ice discharge from 1986 through March 2020. *Earth System Science Data* **12**, 1367–1383.
- McMillan M and 14 others (2014) Rapid dynamic activation of a marine-based Arctic ice cap. *Geophysical Research Letters* **41**(24), 8902–8909.
- McMillan M and 14 others (2016) A high-resolution record of Greenland mass balance. *Geophysical Research Letters* **43**(13), 7002–7010.
- Mernild SH and 7 others (2013) Volume and velocity changes at Mittivakkat Gletscher, southeast Greenland. *Journal of Glaciology* **59**(216), 660–670.
- Miège C and 12 others (2016) Spatial extent and temporal variability of Greenland firn aquifers detected by ground and airborne radars. *Journal of Geophysical Research: Earth Surface* **121**(12), 2381–2398.
- Miller O and 7 others (2018) Direct evidence of meltwater flow within a firn aquifer in southeast Greenland. *Geophysical Research Letters* **45**(1), 207–215.
- Moon T, Joughin I, Smith B and Howat I (2012) 21st-century evolution of Greenland outlet glacier velocities. *Science (New York, N.Y.)* **336**, 576–578.
- Morlighem M and 31 others (2017) BedMachine v3: complete bed topography and ocean bathymetry mapping of Greenland from multibeam echo sounding combined with mass conservation. *Geophysical Research Letters* **44**(21), 11051–11061.
- Morlighem M, Rignot E, Mouginot J, Seroussi H and Larour E (2014) Deeply incised submarine glacial valleys beneath the Greenland ice sheet. *Nature Geoscience* **7**(6), 418–422.
- Motyka RJ and 5 others (2011) Submarine melting of the 1985 Jakobshavn Isbrae floating tongue and the triggering of the current retreat. *Journal of Geophysical Research: Earth Surface* **116**, F01007. doi: [10.1029/2009JF001632](https://doi.org/10.1029/2009JF001632).
- Motyka RJ and 11 others (2017) Asynchronous behavior of outlet glaciers feeding Godthåbsfjord (Nuup Kangerlua) and the triggering of Narsap Sermia's retreat in SW Greenland. *Journal of Glaciology* **63**(238), 288–308.
- Mouginot J and 7 others (2015) Fast retreat of Zachariæ Isstrøm, northeast Greenland. *Science (New York, N.Y.)* **350**(6266), 1357–1361.
- Mouginot J and 8 others (2019) Forty-six years of Greenland Ice Sheet mass balance from 1972 to 201. *Proceedings of the National Academy of Sciences* **116**(19), 9239–9244.
- Murray T and 10 others (2010) Ocean regulation hypothesis for glacier dynamics in southeast Greenland and implications for ice sheet mass changes. *Journal of Geophysical Research: Earth Surface* **115**, F03026. doi: [10.1029/2009JF001522](https://doi.org/10.1029/2009JF001522).
- Murray T and 14 others (2015) Extensive retreat of Greenland tidewater glaciers, 2000–2010. *Arctic, Antarctic, and Alpine Research* **47**(3), 427–447.
- Nick FM, Vieli A, Howat IM and Joughin I (2009) Large-scale changes in Greenland outlet glacier dynamics triggered at the terminus. *Nature Geoscience* **2**(2), 110–114.
- Nienow PW, Sole AJ, Slater DA and Cowton TR (2017) Recent advances in our understanding of the role of meltwater in the Greenland Ice Sheet system. *Current Climate Change Reports* **3**, 330–344.
- Nye JF (1960) The response of glaciers and ice-sheets to seasonal and climatic changes. *Proceedings of the Royal Society A* **256**, 559–584.
- Nye JF (1963) On the theory of the advance and retreat of glaciers. *Geophysical Journal of the Royal Astronomical Society* **7**(4), 431–456.
- Phillips T, Rajaram H, Colgan W, Steffen K and Abdalati W (2013) Evaluation of cryo-hydrologic warming as an explanation for increased ice velocities in the wet snow zone, Sermeq Avannarleq, West Greenland. *Journal of Geophysical Research: Earth Surface* **118**(3), 1241–1256.
- Phillips T, Rajaram H and Steffen K (2010) Cryo-hydrologic warming: a potential mechanism for rapid thermal response of ice sheets. *Geophysical Research Letters* **37**(20), L20503. doi: [10.1029/2010GL044397](https://doi.org/10.1029/2010GL044397).
- Poinar K and 5 others (2015) Limits to future expansion of surface-melt-enhanced ice flow into the interior of western Greenland. *Geophysical Research Letters* **42**(6), 1800–1807.
- Poinar K and 5 others (2017) Drainage of Southeast Greenland firn aquifer water through crevasses to the bed. *Frontiers in Earth Science* **5**(5), <https://doi.org/10.3389/feart.2017.00005>.
- Poinar K, Dow CF and Andrews LC (2019) Long-term support of an active subglacial hydrologic system in Southeast Greenland by firn aquifers. *Geophysical Research Letters* **46**(9), 4772–4781.
- Price SF, Payne AJ, Catania GA and Neumann TA (2008) Seasonal acceleration of inland ice via longitudinal coupling to marginal ice. *Journal of Glaciology* **54**(185), 213–219.
- Price SF, Payne AJ, Howat IM and Smith BE (2011) Committed sea-level rise for the next century from Greenland ice sheet dynamics during the past decade. *Proceedings of the National Academy of Sciences* **108**, 8978–8983.
- Pritchard HD, Arthern RJ, Vaughan DG and Edwards LA (2009) Extensive dynamic thinning on the margins of the Greenland and Antarctic ice sheets. *Nature* **461**(7266), 971–975.
- Riel B, Minchew B and Joughin I (2020) Observing traveling waves in glaciers with remote sensing: new flexible time series methods and application to Sermeq Kujalleq (Jakobshavn Isbræ), Greenland. *The Cryosphere Discussions*, <https://doi.org/10.5194/tc-2020-193>.
- Rignot E, Box JE, Burgess E and Hanna E (2008) Mass balance of the Greenland ice sheet from 1958 to 2007. *Geophysical Research Letters* **35**, L20502.
- Rignot E and Kanagaratnam P (2006) Changes in the velocity structure of the Greenland Ice Sheet. *Science (New York, N.Y.)* **311**(5763), 986–990.
- Rignot E, Velicogna I, van den Broeke MR, Monaghan A and Lenaerts J (2011) Acceleration of the contribution of the Greenland and Antarctic ice sheets to sea level rise. *Geophysical Research Letters* **38**(5), L05503.
- Shepherd A and 45 others (2012) A reconciled estimate of ice-sheet mass balance. *Science (New York, N.Y.)* **338**(6111), 1183–1189.
- Shepherd A and 88 others (2020) Mass balance of the Greenland Ice Sheet from 1992 to 2018. *Nature* **579**, 233–239.
- Simonsen SB and Sørensen LS (2017) Implications of changing scattering properties on Greenland ice sheet volume change from Cryosat-2 altimetry. *Remote Sensing of Environment* **190**, 207–216.
- Smith B and 14 others (2020) Pervasive ice sheet mass loss reflects competing ocean and atmospheric processes. *Science (New York, N.Y.)* **368**(6496), 1239–1242.

- Sole AJ and 6 others** (2011) Seasonal speedup of a Greenland marine-terminating outlet glacier forced by surface melt-induced changes in subglacial hydrology. *Journal of Geophysical Research* **116**, F03014, <http://dx.doi.org/10.1029/2010JF001948>.
- Sole A and 6 others** (2013) Winter motion mediates dynamic response of the Greenland Ice Sheet to warmer summers. *Geophysical Research Letters* **40** (15), 3940–3944.
- Sørensen LS and 5 others** (2018) 25 years of elevation changes of the Greenland Ice Sheet from ERS, Envisat, and CryoSat-2 radar altimetry. *Earth and Planetary Science Letters* **495**, 234–241.
- Stevens LA and 6 others** (2016) Greenland Ice Sheet flow response to runoff variability. *Geophysical Research Letters* **43**(21), 11295–11303.
- Tedstone AJ and 5 others** (2015) Decadal slowdown of a land-terminating sector of the Greenland Ice Sheet despite warming. *Nature* **526**(7575), 692–695.
- Thomas R and 6 others** (2000) Mass balance of the Greenland Ice Sheet at high elevations. *Science (New York, N.Y.)* **289**(5478), 426–428.
- Thomas RH and PARCA Investigators** (2001) Program for Arctic Regional Climate Assessment (PARCA): goals, key findings, and future directions. *Journal of Geophysical Research* **106**(D24), 33691–33705.
- Thomas RH and 5 others** (2003) Investigation of surface melting and dynamic thinning on Jakobshavn Isbrae, Greenland. *Journal of Glaciology* **49**(165), 231–239.
- Thomas RH** (2004) Force-perturbation analysis of recent thinning and acceleration of Jakobshavn Isbrae, Greenland. *Journal of Glaciology* **50**(168), 57–66.
- Thomas RH, Csatho BM, Gogineni S, Jezek KC and Kuivinen K** (1998) Thickening of the western part of the Greenland Ice Sheet. *Journal of Glaciology* **44**(148), 653–658.
- van den Broeke M and 8 others** (2009) Partitioning recent Greenland mass loss. *Science (New York, N.Y.)* **326**, 984–986.
- van der Veen CJ** (2001) Greenland ice sheet response to external forcing. *Journal of Geophysical Research: Atmospheres* **106**(D24), 34047–34058.
- van de Wal RSW and 6 others** (2008) Large and rapid melt-induced velocity changes in the ablation zone of the Greenland Ice Sheet. *Science (New York, N.Y.)* **321**(5885), 111–113.
- van de Wal RSW and 5 others** (2012) Twenty-one years of mass balance observations along the K-transect, west Greenland. *Earth System Science Data* **4**, 31–35.
- van de Wal RSW and 10 others** (2015) Self-regulation of ice flow varies across the ablation area in south-west Greenland. *The Cryosphere* **9**(2), 603–611.
- Vaughan DG and 13 others** (2013) Observations: cryosphere. In Stocker TF and 9 others (eds), *Climate Change 2013: The Physical Science Basis. Contribution of Working Group I to the Fifth Assessment Report of the Intergovernmental Panel on Climate Change*. Cambridge and New York: Cambridge University Press, pp. 317–382.
- Wang W, Li J and Zwally HJ** (2012) Dynamic inland propagation of thinning due to ice loss at the margins of the Greenland ice sheet. *Journal of Glaciology* **58**(210), 734–740.
- Williams JJ, Gourmelen N and Nienow P** (2020) Dynamic response of the Greenland ice sheet to recent cooling. *Scientific Reports* **10**, 1647, <https://doi.org/10.1038/s41598-020-58355-2>.
- Willis MJ and 11 others** (2018) Massive destabilization of an Arctic ice cap. *Earth and Planetary Science Letters* **502**, 146–155.
- Zheng W, Pritchard ME, Willis MJ and Stearns LA** (2019) The possible transition from glacial surge to ice stream on Vavilov ice cap. *Geophysical Research Letters* **46**(23), 13892–13902.
- Zwally H and 11 others** (2011) Greenland ice sheet mass balance: distribution of increased mass loss with climate warming. *Journal of Glaciology* **57**, 88–102.